Renormalization-group analysis of *p*-orbital Bose-Einstein condensates in a square optical lattice

Boyang Liu, Xiao-Lu Yu, and Wu-Ming Liu

Beijing National Laboratory for Condensed Matter Physics, Institute of Physics, Chinese Academy of Sciences, Beijing 100190, China

(Received 6 December 2012; revised manuscript received 12 November 2013; published 3 December 2013)

We investigate the quantum fluctuation effects in the vicinity of the critical point of a *p*-orbital bosonic system in a square optical lattice using the Wilsonian renormalization group, where the *p*-orbital bosons condense at nonzero momenta and display rich phases including both time-reversal symmetry invariant and broken Bose-Einstein condensation states. The one-loop renormalization-group analysis generates corrections to the mean-field phase boundaries. We also show the quantum fluctuations in the *p*-orbital system tend to induce the ordered phase but not destroy it via the Coleman-Weinberg mechanism, which is qualitatively different from the ordinary quantum fluctuation corrections to the mean-field phase boundaries in *s*-orbital systems. Finally, we discuss the observation of these phenomena in the realistic experiment.

DOI: 10.1103/PhysRevA.88.063605 PACS number(s): 03.75.Nt, 05.30.Jp, 67.85.Hj, 67.85.Jk

I. INTRODUCTION

Confining cold atoms in an optical lattice has proven to be an exciting and rich environment for studying many areas of physics [1–5]. However, the ground-state wave functions of single-component bosons are positively defined in the absence of rotation as described in the "no-node" theorem [6], which imposes strong constraint for the feasibility of using boson ground states to simulate many-body physics of interest. One way of circumventing this restriction is to consider the high orbital bands since the "no-node" theorem only applies to ground states [7]. The unconventional Bose-Einstein condensations (BECs) of high orbital bosons exhibit more intriguing properties than the ordinary BECs, including the nematic superfluidity [8,9], orbital superfluidity with spontaneous time-reversal symmetry breaking [10–16], and other exotic properties [17–19]. The theoretic work on the *p*-orbital fermions is also exciting [20–25]. Furthermore, the *p*-orbital and multiorbital superfluidity have been recently realized experimentally by pumping atoms into high orbital bands [3–5,26,27].

Since the *p*-orbital Bose gas exhibits rich phase structures, it is interesting to investigate the quantum fluctuation effects in the vicinity of the critical point in the presence of competing orders. Of particular interest is the quantum fluctuation induced symmetry breaking (QFISB). This phenomenon was first discussed by Coleman and Weinberg [28,29]. They investigated a theory of a massless charged meson coupled to the electrodynamic field by the effective potential method. Starting from a model without symmetry breaking at tree level they found that at one-loop level a new energy minimum was developed away from the origin, thus, the $U(1)$ symmetry of the complex scalar field is spontaneously broken. Independently, Halperin, Lubensky, and Ma [30] discovered the analogous phenomenon in the Ginzburg-Landau theory of superconductor to normal metal transition. Furthermore, this quantum fluctuation induced phase transition is found to be first order [29]. Recently, there have appeared more examples that the symmetry of certain order parameters can be spontaneously broken by the quantum fluctuations in condensed matter systems [31–37]. For instance, in the system of lattice bosons with a three-body hard-core constraint the transitions between the dimer superfluid phase and the conventional atomic superfluid state are proposed to be Ising-like at unit filling and driven first order by fluctuations via the Coleman-Weinberg mechanism at other fractional filling [36,37].

In this paper, we study the *p*-orbital bosonic system in a square optical lattice using renormalization-group (RG) analysis. The spectrum of *p*-orbital bosons in square lattice has two energy minima in the Brillouin zone located at $\vec{K}_X = (\frac{\pi}{a},0)$ for p_x band and $\vec{K}_Y = (0,\frac{\pi}{a})$ for p_y-band, respectively [4,7]. A macroscopic number of the *p*-orbital bosons can condense at these two energy minima. This phenomenon is usually named as "unconventional BEC" [7,14]. At these two band minima the Bloch wave functions are time-reversal invariant and, thus, real valued. Lattice asymmetry favors a ground state that bosons condense at either $\vec{K}_X$ or $\vec{K}_Y$, which is called real BECs. A linear superposition of these two real valued wave functions with a fixed phase difference forms a complex BEC, which is favored by the system with interspecies interactions between p_x and p_y orbital bosons and spontaneously breaks the time-reversal symmetry [7,14]. Since the unconventional BEC is beyond the constraint of "no-node" theorem, it has intriguing properties. In our work we use RG to investigate the quantum phase transitions between the real and complex BEC phases. We find that when the interspecies interactions are turned on the real BEC phases may become unstable and the system can finally flow to the complex BEC phase. The phase transitions for the real BEC phases to the complex BEC phase require the $U(1)$ symmetry breaking of p_x or p_y orbital bosons. This is a phenomenon of quantum-fluctuation-induced phase transition. The phase transitions induced the quantum fluctuations have proven to be in first order [29], which has different scaling behaviors from the second-order ones [38,39]. Based on the recent researches on the quantum criticality in cold-atom physics [40–44], we can propose a method to observe this first-order phase transition in the realistic experiment.

II. THE RENORMALIZATION-GROUP FLOW EQUATIONS AND PHASE DIAGRAMS

The tight-binding model of the *p*-orbital bosons in a square lattice is described by a Hamiltonian as the

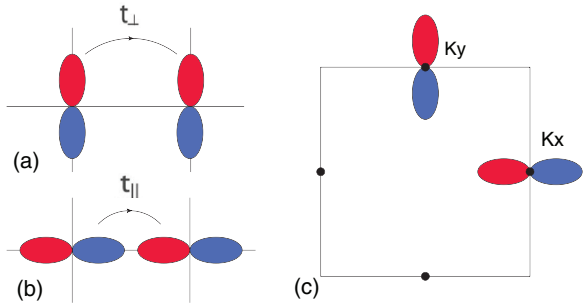

FIG. 1. (Color online) The bonding pattern of p orbitals: (a) the σ bonding and (b) the π bonding. (c) The p-orbital band structure in a square lattice. The band minima are located at $\vec{K}_X = (\frac{\pi}{a},0)$ for the p_x-orbital band, and $\vec{K}_Y = (0,\frac{\pi}{a})$ for the p_y-orbital band, respectively.

following:

$$H = t_{\parallel}\sum_{\langle ij\rangle}\left[p^{\dagger}_{i,\hat{e}_{ij}}p_{j,\hat{e}_{ij}} + \text{H.c.}\right] - t_{\perp}\sum_{\langle ij\rangle}\left[p^{\dagger}_{i,\hat{f}_{ij}}p_{j,\hat{f}_{ij}} + \text{H.c.}\right], \tag{1}$$

where $\hat{e}_{ij}$ and $\hat{f}_{ij}$ are two unit vectors. $\hat{e}_{ij}$ is along the bond orientation between two neighboring sites i and j and $\hat{f}_{ij} = \hat{z}\times\hat{e}_{ij}$. $p_{\hat{e}_{ij}}$ and $p_{\hat{f}_{ij}}$ are the projections of p orbitals along and perpendicular to the bond direction, respectively. The σ bonding $t_{\parallel}$ and the π bonding $t_{\perp}$ describe the hoppings along and perpendicular to the bond direction, which are illustrated in graphs in Figs. 1(a) and 1(b).

This tight-binding model shows that the energy minima are located at half-values of the reciprocal lattice vectors [4,7] as depicted in Fig. 1(c), where $\vec{K}_X = (\frac{\pi}{a},0)$ and $\vec{K}_Y = (0,\frac{\pi}{a})$. The p-orbital bosons can condense at either K_X or K_Y to form a real BEC or both of K_X and K_Y to form a complex BEC. To describe the phase transitions we write down a Landau-Ginzberg theory. The action with the most general interactions is cast as the following:

$$\mathcal{Z} = \int D[\phi^*_1,\phi_1,\phi^*_2,\phi_2]e^{-S[\phi^*_1,\phi_1,\phi^*_2,\phi_2]}, \tag{2}$$

where

$$\begin{aligned}
&S[\phi^*_1,\phi_1,\phi^*_2,\phi_2]\\
&= \int_{-\infty}^{\infty}\frac{d\omega}{2\pi}\int_0^{\Lambda}\frac{d^2k}{(2\pi)^2}\sum_{i=1,2}\phi^*_i(\omega,\vec{k})(-i\omega+\epsilon_k - r_i)\phi_i(\omega,\vec{k})\\
&\quad + \int_{\omega k}^{\Lambda}\Bigg\{\sum_{i=1,2} g_i\phi^*_i(\omega_4,\vec{k}_4)\phi^*_i(\omega_3,\vec{k}_3)\phi_i(\omega_2,\vec{k}_2)\phi_i(\omega_1,\vec{k}_1)\\
&\quad + g_3\phi^*_2(\omega_4,\vec{k}_4)\phi^*_1(\omega_3,\vec{k}_3)\phi_1(\omega_2,\vec{k}_2)\phi_2(\omega_1,\vec{k}_1)\\
&\quad + g_4[\phi^*_1(\omega_4,\vec{k}_4)\phi^*_1(\omega_3,\vec{k}_3)\phi_2(\omega_2,\vec{k}_2)\phi_2(\omega_1,\vec{k}_1) + \text{H.c.}]\Bigg\},
\end{aligned} \tag{3}$$

where ϕ_1 and ϕ_2 describe the condensate order parameters at K_X and K_Y, respectively. Here we used a short-handed notation $\int_{\omega k}^{\Lambda} = \prod_{i=1}^{4}\int_{-\infty}^{\infty}\frac{d\omega_i}{2\pi}\int_0^{\Lambda}\frac{d^2k_i}{(2\pi)^2}(2\pi)^2\delta(\vec{k}_4+\vec{k}_3-\vec{k}_2-\vec{k}_1)(2\pi)\delta(\omega_4+\omega_3-\omega_2-\omega_1)$. A cutoff Λ is given to the momentum space since this is a low-energy effective theory. Terms with g_1 and g_2 are the intraspecies interactions of p_x and p_y orbital bosons. Terms with g_3 and g_4 describes the interspecies interactions. The g_4 term can rise in this high orbital model as an Umklapp scattering process since the momentum transfer is $\pm 2(\vec{K}_X - \vec{K}_Y)$, which equals to the reciprocal lattice vectors [7,14].

In contrast to the mean-field theory where certain order parameter is presumably defined, the renormalization-group analysis treats various instabilities on an equal footing without assuming any specific order parameters. Here we implement the momentum-shell renormalization-group method to study the running of various parameters. Following the Wilson's approach [45] the renormalization-group transformation involves three steps: (i) integrating out all momenta between Λ/s and Λ, for tree-level analysis just discarding the part of the action in this momentum shell; (ii) rescaling frequencies and the momenta as $(\omega,k)\to(s^{[\omega]}\omega,sk)$ so that the cutoff in k is once again at $\pm\Lambda$; and finally (iii) rescaling fields $\phi\to s^{[\phi]}\phi$ to keep the free-field action S_0 invariant.

In order to perform the first step of Wilson's approach in the one-loop level, we need to split the fields into "slow modes" $\phi_{i<}(\omega,\vec{k})$ and "fast modes" $\phi_{i>}(\omega,\vec{k})$. Then we have

$$\phi_i(\omega,\vec{k}) = \phi_{i<}(\omega,\vec{k}) + \phi_{i>}(\omega,\vec{k}), \tag{4}$$

where

$$\begin{aligned}
&\phi_{i<}(\omega,\vec{k}) \quad \text{for} \quad 0<|k|<\Lambda/s,\\
&\phi_{i>}(\omega,\vec{k}) \quad \text{for} \quad \Lambda/s<|k|<\Lambda.
\end{aligned} \tag{5}$$

The partition function now can be written as

$$\begin{aligned}
\mathcal{Z} = &\int D[\phi^*_{1<},\phi_{1<},\phi^*_{2<},\phi_{2<}]e^{-S[\phi^*_{1<},\phi_{1<},\phi^*_{2<},\phi_{2<}]}\\
&\times\int D[\phi^*_{1>},\phi_{1>},\phi^*_{2>},\phi_{2>}]\\
&\times e^{-S_0[\phi^*_{1>},\phi_{1>},\phi^*_{2>},\phi_{2>}]-S_I[\phi^*_{1<},\phi_{1<},\phi^*_{2<},\phi_{2<},\phi^*_{1>},\phi_{1>},\phi^*_{2>},\phi_{2>}]}.
\end{aligned} \tag{6}$$

We next construct an effective action by integration over the fast fields. To the one-loop order, one obtains

$$\begin{aligned}
&e^{-S_{\text{eff}}[\phi^*_{1<},\phi_{1<},\phi^*_{2<},\phi_{2<}]}\\
&= e^{-S[\phi^*_{1<},\phi_{1<},\phi^*_{2<},\phi_{2<}]}\\
&\quad\times\exp[-\langle S_I[\phi^*_{1<},\phi_{1<},\phi^*_{2<},\phi_{2<},\phi^*_{1>},\phi_{1>},\phi^*_{2>},\phi_{2>}]\rangle_>\\
&\quad + \tfrac{1}{2}\langle S_I[\phi^*_{1<},\phi_{1<},\phi^*_{2<},\phi_{2<},\phi^*_{1>},\phi_{1>},\phi^*_{2>},\phi_{2>}]^2\rangle_>],
\end{aligned} \tag{7}$$

where $\langle\cdots\rangle_>$ denotes the average over the fast fluctuations. We perform the integrals over the fast modes by evaluating the appropriate Feynman diagrams contributing to the renormalization of the vertices of interest. The one-loop Feynman graphs contributing to the renormalization are shown in Fig. 2.

One finds that the parameters r_1 and r_2 scale according to the following relations up to one-loop order:

$$\begin{aligned}
\frac{d\tilde{r}_1}{d\ell} &= 2\tilde{r}_1 + 4\tilde{g}_1\cdot\theta(\tilde{r}_1-1/2) + \tilde{g}_3\cdot\theta(\tilde{r}_2-1/2),\\
\frac{d\tilde{r}_2}{d\ell} &= 2\tilde{r}_2 + 4\tilde{g}_2\cdot\theta(\tilde{r}_2-1/2) + \tilde{g}_3\cdot\theta(\tilde{r}_1-1/2).
\end{aligned} \tag{8}$$

In above equations we defined the dimensionless parameters as $\tilde{r}_i = r_i m/\Lambda^2$ and $\tilde{g}_i = g_i m/(2\pi)$. The θ functions in the flow

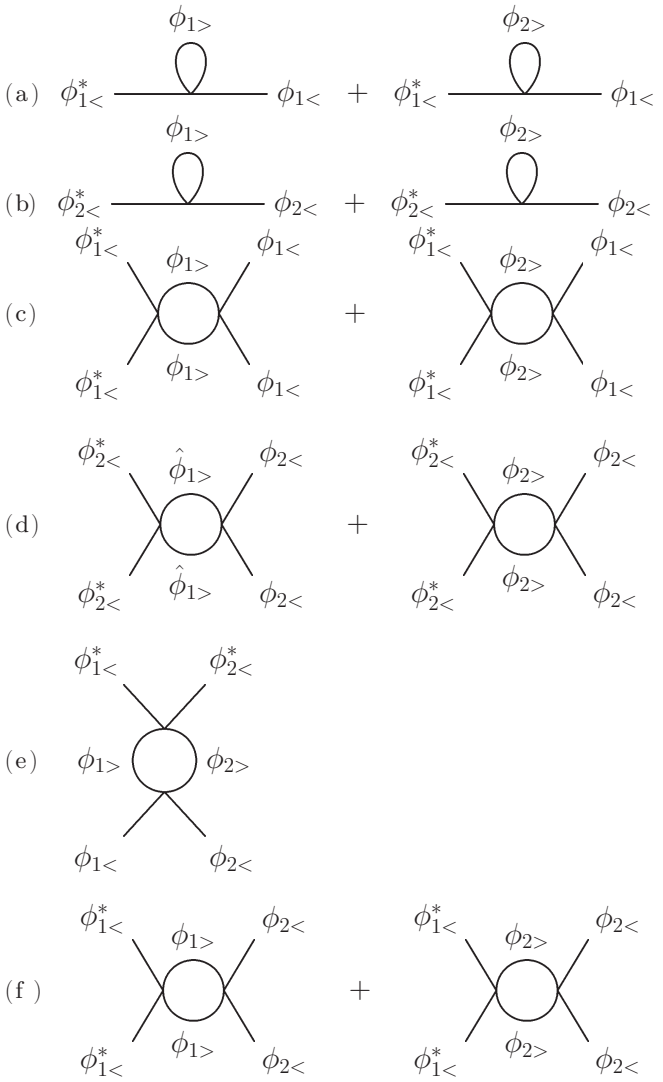

FIG. 2. The one-loop Feynman graphs contributing to the renormalization of (a) the parameter r_1, (b) the parameter r_2, (c) the interaction g_1, (d) the interaction g_2, (e) the interaction g_3, and (f) the interaction g_4.

equations of $\tilde{r}_1$ and $\tilde{r}_2$ are from ω integrations in the one-loop calculations, where we have $\theta(\tilde{r}-1/2)=\int_{-\infty}^{+\infty}\frac{d\omega}{2\pi}\frac{e^{i\omega 0^+}}{i\omega-(1/2-\tilde{r})}$. Notice that we introduced the factor $e^{i\omega 0^+}$ into the ω integral otherwise the integral over ω does not converge [46]. Most of the studies investigated the behaviors around the critical point, then these contributions can be ignored at zero temperature [47,48]. However, in our case the running behaviors of r_1 and r_2 to $+\infty$ or $-\infty$ are used as the criteria of which phase the system will fall into. Therefore, we have to take these contributions into account. They will give severe influence to the running of $\tilde{r}_1$ and $\tilde{r}_2$. The flow equations of the coupling constants are as follows:

$$\begin{aligned}\frac{d\tilde{g}_1}{d\ell}&=-2\tilde{g}_1^2-2\tilde{g}_4^2,\quad \frac{d\tilde{g}_2}{d\ell}=-2\tilde{g}_2^2-2\tilde{g}_4^2,\\ \frac{d\tilde{g}_3}{d\ell}&=-\tilde{g}_3^2,\quad \frac{d\tilde{g}_4}{d\ell}=-2\tilde{g}_1\tilde{g}_4-2\tilde{g}_2\tilde{g}_4.\end{aligned}\tag{9}$$

All the coupling constants with positive initial values are marginally irrelevant. For example, $\tilde{g}_3$ can be solved as $\tilde{g}_3(\ell)=\frac{\tilde{g}_3(0)}{1+\tilde{g}_3(0)\ell}$. It approaches to zero as the length scale ℓ goes to infinity. However, it does not imply that we can ignore these irrelevant coupling constants. This is because the small $\tilde{g}_i$ will generate small contributions to $\tilde{r}_i$, which will then quickly grow under the renormalization. As discussed by Shankar [46], an irrelevant operator can modify the flow of the relevant couplings before it renormalizes to zero.

The running parameters $\tilde{r}_1(\ell)$ and $\tilde{r}_2(\ell)$ are relevant and can be solved numerically from Eq. (8). We find that in regions of $\tilde{r}_1(0)\geqslant\frac{1}{2}\&\tilde{r}_2(0)\geqslant\frac{1}{2}$ the solutions are

$$\begin{aligned}\tilde{r}_1(\ell)&=e^{2\ell}\left[\tilde{r}_1(0)+\int_0^\ell e^{-2t}(4\tilde{g}_1(t)+\tilde{g}_3(t))dt\right],\\ \tilde{r}_2(\ell)&=e^{2\ell}\left[\tilde{r}_2(0)+\int_0^\ell e^{-2t}(4\tilde{g}_2(t)+\tilde{g}_3(t))dt\right].\end{aligned}\tag{10}$$

In this region the initial values $\tilde{r}_1(0)$ and $\tilde{r}_2(0)$ and the one-loop level contributions are all positive since all the interactions are repulsive. Thus, $\tilde{r}_1(\ell)$ and $\tilde{r}_2(\ell)$ are both running to positive infinity fast due to the exponential prefactor. The one-loop contributions do not change the flow directions of the chemical potentials. The running directions of $\tilde{r}_1(\ell)$ and $\tilde{r}_2(\ell)$ are completely determined by their initial values. If the initial values are positive or negative, they finally flow to positive or negative infinity. In the region of $\tilde{r}_1(0)\geqslant\frac{1}{2}\&\tilde{r}_2(0)<\frac{1}{2}$ the solutions are

$$\begin{aligned}\tilde{r}_1(\ell)&=e^{2\ell}\left[\tilde{r}_1(0)+\int_0^\ell e^{-2t}4\tilde{g}_1(t)dt\right],\\ \tilde{r}_2(\ell)&=e^{2\ell}\left[\tilde{r}_2(0)+\int_0^\ell e^{-2t}\tilde{g}_3(t)dt\right].\end{aligned}\tag{11}$$

In the region of $\tilde{r}_1(0)<\frac{1}{2}\&\tilde{r}_2(0)\geqslant\frac{1}{2}$ the solutions are

$$\begin{aligned}\tilde{r}_1(\ell)&=e^{2\ell}\left[\tilde{r}_1(0)+\int_0^\ell e^{-2t}\tilde{g}_3(t)dt\right],\\ \tilde{r}_2(\ell)&=e^{2\ell}\left[\tilde{r}_2(0)+\int_0^\ell e^{-2t}4\tilde{g}_2(t)dt\right].\end{aligned}\tag{12}$$

Different from the first region, in these two regions $\tilde{r}_1(0)$ or $\tilde{r}_2(0)$ can be negative. The positive contributions from the one-loop graphs may qualitatively change the running behaviors of $\tilde{r}_1(\ell)$ or $\tilde{r}_2(\ell)$. That is, even if $\tilde{r}_1(\ell)$ or $\tilde{r}_2(\ell)$ runs to negative infinity at the tree level, the positive one-loop contributions can make $\tilde{r}_1(\ell)$ or $\tilde{r}_2(\ell)$ go to positive infinity eventually. The system will finally end up in a different phase. This generates critical lines in these two regions, which are determined by conditions $\tilde{\mu}_2(0)+\int_0^\infty e^{-2t}\frac{\tilde{g}_3(0)}{1+\tilde{g}_3(0)t}dt=0$ and $\tilde{\mu}_1(0)+\int_0^\infty e^{-2t}\frac{\tilde{g}_3(0)}{1+\tilde{g}_3(0)t}dt=0$. However, in other regions the running directions of $\tilde{r}_1(\ell)$ and $\tilde{r}_2(\ell)$ can eventually be changed by the one-loop corrections from the interaction couplings, even if they renormalize to zero. For instance, in Fig. 3 we start the running of $\tilde{r}_1(\ell)$ from a negative initial value.

As we vary the interaction coupling $\tilde{g}_3(0)$ from 0.3 to 0.8 we observe that the running of $\tilde{r}_1(\ell)$ can finally be changed from the negative to the positive direction. That is, even if $\tilde{r}_1(\ell)$ runs to negative infinity at the tree level, the positive

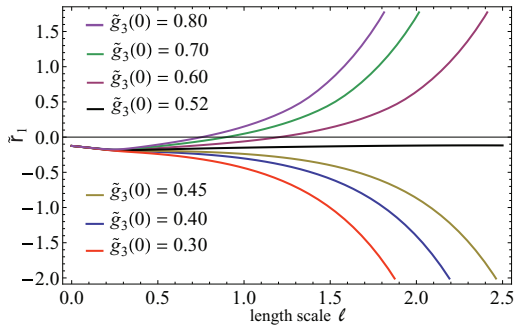

FIG. 3. (Color online) The flow directions of parameter $\tilde{r}_1(\ell)$ with different interaction coupling $\tilde{g}_3(0)$. As $\tilde{g}_3(0)$ is increased the running direction of $\tilde{r}_1(\ell)$ changes from negative infinity to positive infinity. The system can finally flow to a condensed phase. The initial values of the parameters are $\tilde{r}_1(0) = -0.125$, $\tilde{r}_2(0) = 0.3$ and $\tilde{g}_1(0) = \tilde{g}_2(0) = \tilde{g}_4(0) = 0.1$.

one-loop contributions can make $\tilde{r}_1(\ell)$ go to positive infinity eventually. The system will finally end up in a different phase. In region of $\tilde{r}_1(0) < \frac{1}{2} \& \tilde{r}_2(0) < \frac{1}{2}$ the solutions are

$$\tilde{r}_1(\ell) = \tilde{r}_1(0)e^{2\ell}, \quad \tilde{r}_2(\ell) = \tilde{r}_2(0)e^{2\ell}. \tag{13}$$

In this region it is easy to see the running behaviors are totally determined by the tree-level scaling. However, with certain initial values $\tilde{r}_1(\ell)$ and $\tilde{r}_2(\ell)$ can finally flow to the second or the third region and then continuously flow to positive infinity or negative infinity, there are also critical lines in this region.

Based on the numerical calculations the phase diagrams can be drawn in Fig. 4. The four phases are determined by the flow directions of $\tilde{r}_1(\ell)$ and $\tilde{r}_2(\ell)$ as $\ell \to \infty$.

(I) Complex BEC: $\tilde{r}_1(\ell) \to +\infty$ and $\tilde{r}_2(\ell) \to +\infty$,
(II) Real BEC 1: $\tilde{r}_1(\ell) \to +\infty$ and $\tilde{r}_2(\ell) \to -\infty$,
(III) Real BEC 2: $\tilde{r}_1(\ell) \to -\infty$ and $\tilde{r}_2(\ell) \to +\infty$,
(IV) No BEC: $\tilde{r}_1(\ell) \to -\infty$ and $\tilde{r}_2(\ell) \to -\infty$.

We find that without interspecies interactions the complex BEC phase is confined in the first quadrant of the phase diagram as shown in Fig. 4(a). However, as we turn on the interspecies interactions the complex phase is enlarged into the second and fourth quadrants as shown in Figs. 4(b)–4(d). Comparing the four phase diagrams in Fig. 4, we see that as the interspecies interaction $\tilde{g}_3(0)$ becomes stronger the complex BEC phase get enhanced. That is, certain region of real BEC phases become unstable when the interspecies interactions are turned on and the system finally flows to the complex BEC phase. These interactions give rise to an instability from the real BEC phase to the complex BEC phase. The phase transitions for the real BEC phases to the complex BEC phase require the $U(1)$ symmetry breaking of p_x- or p_y-orbital bosons. Given that $\tilde{g}_3(0)$ is small, we can obtain the approximate expressions of the two boundaries. Boundary 1 is

$$\tilde{r}_2(0) = -\frac{\tilde{r}_1(0)\tilde{g}_3(0)}{1 - \frac{1}{2}\ln(2\tilde{r}_1(0)) \cdot \tilde{g}_3(0)} \quad \text{for} \quad 0 < \tilde{r}_1(0) < \frac{1}{2},$$
$$\tilde{r}_2(0) = -\frac{\tilde{g}_3(0)}{2} \quad \text{for} \quad \tilde{r}_1(0) > \frac{1}{2}. \tag{14}$$

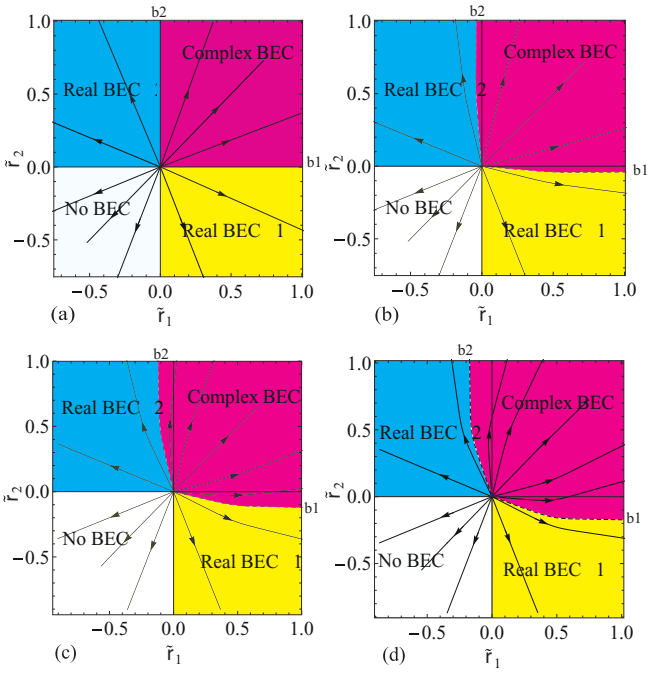

FIG. 4. (Color online) Phase diagrams of the p-orbital boson system. Four phases are determined by the flow directions of the parameters $\tilde{r}_1$ and $\tilde{r}_2$ under the renormalization-group transformation. In the complex BEC phase $\tilde{r}_1(\ell)$ and $\tilde{r}_2(\ell)$ run to positive infinities, which represents that both p_x and p_y orbital bosons condense. In the real BEC 1 (or 2) phase the p_x (or p_y) orbital boson condenses and the other one does not. In the no-BEC phase neither of the two orbital bosons condense. The initial values of the couplings are $\tilde{g}_1(0) = \tilde{g}_2(0) = \tilde{g}_4(0) = 0.1$ for all of the four diagrams. The interspecies interaction coupling $\tilde{g}_3(0)$ between the p_x and p_y orbital bosons is set to 0,0.1,0.3, and 0.5 for graphs (a), (b), (c), and (d), respectively. "b1" and "b2" denote boundary 1 and boundary 2 between the real and complex BEC phases.

Boundary 2 is

$$\tilde{r}_1(0) = -\frac{\tilde{r}_2(0)\tilde{g}_3(0)}{1 - \frac{1}{2}\ln(2\tilde{r}_2(0)) \cdot \tilde{g}_3(0)} \quad \text{for} \quad 0 < \tilde{r}_2(0) < \frac{1}{2},$$
$$\tilde{r}_1(0) = -\frac{\tilde{g}_3(0)}{2} \quad \text{for} \quad \tilde{r}_2(0) > \frac{1}{2}. \tag{15}$$

They are indicated by "$b1$" and "$b2$" in Fig. 4.

III. QUANTUM-FLUCTUATION-INDUCED SYMMETRY BREAKING

The mean-field results of the phase transition was derived by constructing a Ginzburg-Landau theory in Ref. [14]. However, our renormalization-group analysis gives some qualitative differences: (I) In the mean-field analysis the boundary conditions between the real and complex BEC phases depend on the self-interaction couplings g_1 and g_2. However, these two couplings do not affect the phase boundaries in our results. The quantum phase transition is purely induced by the interspecies interaction between the p_x- and p_y-orbital bosons in RG analysis. (II) At one-loop level the g_4 term does not give any contributions to the flow equations of parameter r_1 and r_2. It can get involved in higher order calculations. For instance, g_4

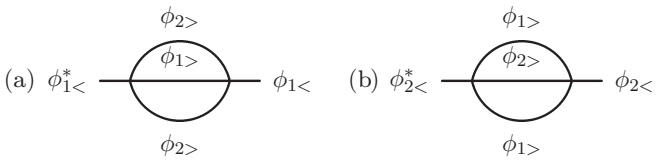

FIG. 5. The Feynman diagrams of the two-loop corrections to the parameter (a) r_1 and (b) r_2. ϕ_1 and ϕ_2 are the boson fields defined in Eq. (1).

term can generate corrections to the boundaries "b1" and "b2" at the two-loop level through the sunrise graphs in Fig. 5.

However, in mean-field analysis the phase boundaries depend on both g_4 and g_3. This difference originates from the starting points of the two analyses. The g_4 term explicitly breaks the original $U(1) \times U(1)$ symmetry to $U_D(1)$ symmetry, where the index "D" denotes "Diagonal," and leads to a fixed phase difference between the two fields ϕ_1 and ϕ_2. The mean-field analysis starts from this symmetry breaking phase. Hence, the complex phase in mean field is a coherent superposition of the two ground states. However, our renormalization-group analysis starts from the normal phase and focuses on the effects of the quantum fluctuations. In this case the g_4 term does not show its contributions up to the one-loop level. Our complex phase is just a incoherent mixture of the two ground states. (III) The comparison of the phase diagrams of the renormalization-group analysis and mean-field theory can be illustrated in Fig. 6.

In order to compare the two phase diagrams with the same circumstance we set $g_4 = 0$ in the mean-field phase diagram. The expressions of the mean-field phase boundaries are $\frac{\tilde{r}_2}{\tilde{r}_1} = \frac{2\tilde{g}_2}{\tilde{g}_3}$ and $\frac{\tilde{r}_2}{\tilde{r}_1} = \frac{\tilde{g}_3}{2\tilde{g}_1}$ [14]. In Fig. 6 it is obvious to see that the crucial difference is that the complex BEC phase is enlarged and the real BEC phase is suppressed in the RG phase diagram.

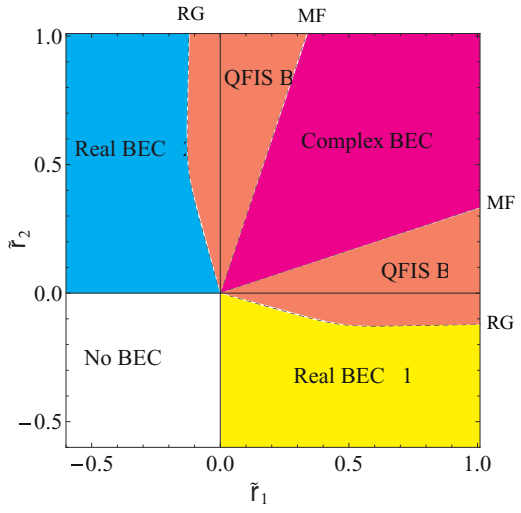

FIG. 6. (Color online) Comparison of phase boundaries from the renormalization-group analysis and the mean-field analysis. "MF" and "RG" indicate the boundaries from the mean-field and renormalization-group analyses, respectively. The complex BEC phase in renormalization-group analysis is larger than the one from mean-field theory by a region named "QFISB." The coupling constants are $\tilde{g}_1 = \tilde{g}_2 = 0.5$, $\tilde{g}_3 = 0.3$, and $\tilde{g}_4 = 0$.

In essence, the above differences can be explained as effects of the "quantum-fluctuation-induced symmetry breaking." The phase transitions from real BEC to complex BEC phase indicate the $U(1)$ symmetry breakdown of field ϕ_1 or ϕ_2. Mean-field description of the symmetry breaking is based on semiclassical approximation. In other words, it is a tree-level result. When we take into account the quantum fluctuation, the one-loop corrections can significantly change the model parameters and make some region of the real BEC phase become unstable. In Fig. 6 these regions are labeled by "QFISB." The original QFISB effect was studied using the effective potential method [28]. Our work reaches a qualitatively analogous result using renormalization-group analysis.

Of particular importance is that this phenomenon has a qualitative difference from the ordinary quantum corrections to the mean-field results. For instance, in an s-orbital system the phase transition is described by the ϕ^4 theory. The renormalization-group calculations show that the system may flow from an ordered phase to a disordered phase when the quantum fluctuations are taken into account. That is, the quantum fluctuations tend to destroy the ordered phase but not induce it [49]. However, in our p-orbital system the ordered phase of one type of orbital bosons may be induced by the quantum fluctuations from the interactions with the other type of orbital bosons. In Fig. 4 we show that the system in the disordered phase (real BEC phase) may flow to the ordered phase (complex BEC phase) under the RG transformations. Furthermore, in the ϕ^4 theory of the s-orbital system the phase transition occurs at the Wilson-Fisher fixed point with finite values of couplings. The transition is second order. However, in our work r_1 and r_2 are both runaway trajectories. They flow to $+\infty$ or $-\infty$. This infinity is characteristic of the first-order phase transition. Actually, the quantum-fluctuation-induced phase transition has proven to be first order in the effective potential method [29].

IV. FINITE TEMPERATURE SCALING AND EXPERIMENTAL PROPOSAL

In order to give a realistic experimental proposal to observe this quantum-fluctuation-induced first-order phase transition we investigate the finite temperature scaling behaviors of our system. In the vicinity of the quantum critical points the observables obey universal scaling relations. An interesting feature of the scaling approach is that it allows one to determine the singular behavior of the physics quantities of interests as a function of temperature at criticality. For instance, we consider the system undergoes a phase transition between the "complex BEC" phase and the "real BEC 2" phase. To discuss this transition, it is convenient to introduce a parameter $\delta \equiv r_1 - r_{1c}$ to measure the distance to the transition. Then, the finite temperature scaling behavior of the free energy density near the critical line "b1" can be described as the following:

$$f(\delta, T) \sim |\delta|^{\nu(d+z)} \tilde{f}(T/|\delta|^{\nu z}), \tag{16}$$

where d is the special dimension of the system, ν is the correlation length exponent, and z is the dynamic exponent. $\tilde{f}(u)$ is a universal scaling function, which approaches a constant as $u \to 0$. Thus, the critical temperature T_c vanishes

like $T_c = u_c \delta^{z\nu}$ for small δ. A general discussion shows that the scaling behaviors near a first-order phase transition are characterized by the scaling exponents such as $\beta = 0$, $\alpha = \gamma = 1$, and $\nu = 1/(d+z)$ [38,39]. In our case, the dynamic exponent is $z = 2$ and the system dimension is $d = 2$. Thus, the correlation length exponent is $\nu = 1/(d+z) = 1/4$. The scaling of the critical temperature is $T_c \sim \sqrt{|\delta|}$.

Recently, several schemes were proposed to determine the critical properties in cold-atom systems by extracting the universal scaling functions from the atomic density profiles [40–42]. The experimental observations of quantum critical behavior of ultracold atoms have also been reported [43,44]. The study of quantum criticality in cold-atom systems is based on *in situ* density measurements [40–42,44]. The density can be cast as $n(\mu,T) - n_r(\mu,T) = T^{\frac{d}{z}+1-\frac{1}{z\nu}} G(\frac{\mu-\mu_c}{T^{1/z\nu}})$, where μ_c is the critical value of the chemical potential, n_r is the regular part of the density, and $G(x)$ is a universal function describing the singular part of the density. Following the scheme developed by Zhou and Ho [40] we can locate the quantum critical point μ_c and then plot the "scaled density" $A(\mu,T)$ versus $(\mu-\mu_c)/T^{\frac{1}{\nu z}}$, where

$$A(\mu,T) \equiv T^{-\frac{d}{z}-1+\frac{1}{z\nu}}(n(\mu,T) - n_r). \tag{17}$$

The scaled density curves for all temperatures will collapse into a single curve. Then we can utilize this curve of scaling function to test the critical scaling law based on the expected critical exponents.

Within the above scheme we consider the observation of the quantum-fluctuation-induced first-order phase transition in the p-orbital bosonic system. One leading candidate to observe this phenomenon is ^{87}Rb atoms in a bipartite optical square lattice [4]. The optical potential can be constructed by crossing two laser beams with wavelength $\lambda = 1064$ nm and $1/e^2$ radius $w_0 = 100r$ m. The optical potential reads $-\frac{V_0}{4} e^{-\frac{2z^2}{w_0^2}} |\eta[(\hat{z}\cos\alpha + \hat{y}\sin\alpha)e^{ikx} + \epsilon\hat{z}e^{-ikx}] + e^{i\theta}\hat{z}(e^{iky} + \epsilon e^{-iky})|^2$. $\epsilon < 1$ and $\eta < 1$ describe the imperfect reflection and transmission efficiencies, respectively. The typical values of ϵ and η are $\epsilon \approx 0.81$ and $\eta \approx 0.95$. A BEC of 2×10^5 ^{87}Rb atoms (in the $F = 2, m_F = 2$ state) is produced in the optical trap. With V_0 set to $V_0/E_{\rm rec} = 6.2$ the excitation of the p-orbital band can be obtained by ramping θ from 0.38π to 0.53π within 0.2 ms. The initial values of the parameters r_1 and r_2 can be properly chosen by tuning α, which is the angle between the z axis and the linear polarization of the incident beam.

We can fine tune α to zero so that the system is prepared in the vicinity of the critical line "b1" in Fig. 6. By taking *in situ* measurement the density profile of the system can be extracted. Following Zhou's and Ho's scheme [40] we can draw a curve of the universal scaling function. If the system undergos a first-order phase transition the scaled density will be in the form of $A(\mu,T) = n(\mu,T) - n_r$ near the first-order QCP, where we have used $z = 2, d = 2$, and $\nu = \frac{1}{4}$ in Eq. (17). To compare this phase transition with the second-order phase transition we also calculate the scaled density near the second-order QCP, which belongs to the two-dimensional XY universality class with critical exponents $z = 2$ and $\nu = 1/2$. Then the scaled density is $A(\mu,T) = T^{-1}(n(\mu,T) - n_r)$. By testing which form the measured scaled density obeys we can determine whether the phase transition is in first or second order.

V. CONCLUSION

In summary, we have investigated the quantum phase transitions of the p-orbital boson gas in a square optical lattice using the renormalization-group method. We find that phase transitions from the real BEC phases to the complex BEC phase can be induced by quantum fluctuations from the interactions between p_x- and p_y-orbital bosons. The transition indicates the $U(1)$ symmetry breaking of p_x- and p_y-orbital bosons. This is a phenomenon different from the s-orbital case, where the quantum fluctuations tend to destroy the ordered phase but not induce it. We find that this effect is purely induced by the interspecies interactions. Our renormalization-group analysis also indicates that this is a first-order phase transition. Finally, we gave an experimental proposal to observe this phenomenon in the realistic experiment.

ACKNOWLEDGMENTS

It is a pleasure to thank Congjun Wu for suggesting the problem to us. We would also like to thank Jiangping Hu and Anchun Ji for useful discussions. This work is supported by the NKBRSFC under Grants No. 2012CB821400, No. 2011CB921502, and No. 2012CB821305, and NSFC under Grants No. 1190024, No. 61227902 and No. 61378017.

[1] D. Jaksch, C. Bruder, J. I. Cirac, C. W. Gardiner, and P. Zoller, Phys. Rev. Lett. **81**, 3108 (1998).
[2] M. Greiner, O. Mandel, T. Esslinger, T. W. Hänsch, and I. Bloch, Nature (London) **415**, 39 (2002).
[3] T. Müller, S. Fölling, A. Widera, and I. Bloch, Phys. Rev. Lett. **99**, 200405 (2007).
[4] G. Wirth, M. Ölschläger, and A. Hemmerich, Nature Phys. **7**, 147 (2011).
[5] P. Soltan-Panahi, D. Lühmann, J. Struck, P. Windpassinger, and K. Sengstock, Nature Phys. **8**, 71 (2012).
[6] R. P. Feynman, *Statistical Mechanics, A Set of Lectures* (Addison-Wesley, Boston, 1972).
[7] C. Wu, Mod. Phys. Lett. B **23**, 1 (2009).
[8] A. Isacsson and S. M. Girvin, Phys. Rev. A **72**, 053604 (2005).
[9] C. Xu and M. P. A. Fisher, Phys. Rev. B **75**, 104428 (2007).
[10] W. V. Liu and C. Wu, Phys. Rev. A **74**, 013607 (2006).
[11] C. Wu, W. V. Liu, J. E. Moore, and S. Das Sarma, Phys. Rev. Lett. **97**, 190406 (2006).
[12] V. M. Stojanović, C. Wu, W. V. Liu, and S. Das Sarma, Phys. Rev. Lett. **101**, 125301 (2008).
[13] A. B. Kuklov, Phys. Rev. Lett. **97**, 110405 (2006).
[14] Z. Cai and C. Wu, Phys. Rev. A **84**, 033635 (2011).
[15] M. Lewenstein and W. V. Liu, Nature Phys. **7**, 101 (2011).
[16] J. P. Martikainen and J. Larson, Phys. Rev. A **86**, 023611 (2012).
[17] C. Wu, D. Bergman, L. Balents, and S. Das Sarma, Phys. Rev. Lett. **99**, 070401 (2007).

[18] V. W. Scarola and S. DasSarma, Phys. Rev. Lett. **95**, 033003 (2005).
[19] X. Li, Z. Zhang, and W. V. Liu, Phys. Rev. Lett. **108**, 175302 (2012).
[20] C. Wu, Phys. Rev. Lett. **101**, 186807 (2008).
[21] K. Wu and H. Zhai, Phys. Rev. B **77**, 174431 (2008).
[22] E. Zhao and W. V. Liu, Phys. Rev. Lett. **100**, 160403 (2008).
[23] S. Zhang, H. H. Hung, and C. Wu, Phys. Rev. A **82**, 053618 (2010).
[24] X. Li, E. Zhao, and W. V. Liu, Phys. Rev. A **83**, 063626 (2011).
[25] M. Zhang, H. H. Hung, C. Zhang, and C. Wu, Phys. Rev. A **83**, 023615 (2011).
[26] J. Sebby-Strabley, M. Anderlini, P. S. Jessen, and J. V. Porto, Phys. Rev. A **73**, 033605 (2006).
[27] M. Ölschläger, G. Wirth, and A. Hemmerich, Phys. Rev. Lett. **106**, 015302 (2011).
[28] S. Coleman and E. Weinberg, Phys. Rev. D **7**, 1888 (1973).
[29] D. J. Amit, *Field Theory, the Renormalization Group and Critical Phenomena* (World Scientific, Singapore, 1984).
[30] B. I. Halperin, T. C. Lubensky, and S.-K. Ma, Phys. Rev. Lett. **32**, 292 (1974).
[31] M. A. Continentino and A. S. Ferreira, Physica A **339**, 461 (2004).
[32] A. S. Ferreira, M. A. Continentino, and E. C. Marino, Phys. Rev. B **70**, 174507 (2004).
[33] Y. Qi and C. Xu, Phys. Rev. B **80**, 094402 (2009).
[34] A. J. Millis, Phys. Rev. B **81**, 035117 (2010).
[35] Jian-Huang She, Jan Zaanen, Alan R. Bishop, and Alexander V. Balatsky, Phys. Rev. B **82**, 165128 (2010).
[36] S. Diehl, M. Baranov, A. J. Daley, and P. Zoller, Phys. Rev. Lett. **104**, 165301 (2010).
[37] Lars Bonnes and Stefan Wessel, Phys. Rev. Lett. **106**, 185302 (2011).
[38] B. Nienhuis and N. Nauenberg, Phys. Rev. Lett. **35**, 477 (1975).
[39] M. E. Fisher and A. N. Berker, Phys. Rev. B **26**, 2507 (1982).
[40] Q. Zhou and T.-L. Ho, Phys. Rev. Lett. **105**, 245702 (2010).
[41] K. R. A. Hazzard and E. J. Mueller, Phys. Rev. A **84**, 013604 (2011).
[42] X. Zhang, C.-L. Hung, S.-K. Tung, N. Gemelke, and C. Chin, New J. Phys. **13**, 045011 (2011).
[43] T. Donner, S. Ritter, T. Bourdel, A. Öttl, M. Köhl, and T. Esslinger, Science **315**, 1556 (2007).
[44] X. Zhang, C.-L. Hung, S.-K. Tung, and C. Chin, Science **335**, 1070 (2012).
[45] K. G. Wilson and J. B. Kogut, Phys. Rep. **12**, 75 (1974).
[46] R. Shankar, Rev. Mod. Phys. **66**, 129 (1994).
[47] S. Sachdev, T. Senthil, and R. Shankar, Phys. Rev. B **50**, 258 (1994).
[48] S. Sachdev and E. R. Dunkel, Phys. Rev. B **73**, 085116 (2006).
[49] A. Altland and B. Simons, *Condensed Matter Field Theory* (Cambridge University Press, Cambridge, 2010).